A

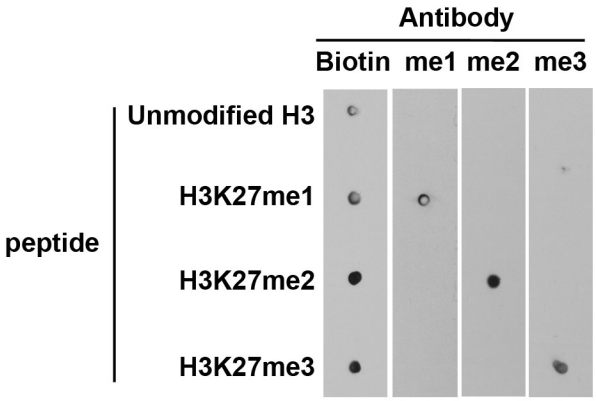

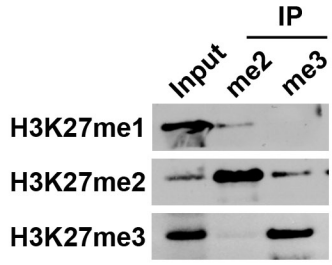

B

ChIP-seq	Cell type	# of unique reads	# of peaks
H3K27me3	ES-WT	30867008	21826
H3K27me3	ES-WT	65907766	33272
H3K27me3	ES-Y641F	55966605	36525
H3K27me3	ES-Y641F	55184754	31433
H3K27me3	24h diff-WT	41951103	26752
H3K27me3	24h diff-WT	98202471	34378
H3K27me3	EB8-WT	50798469	17309
H3K27me2	ES-WT	41803365	30722
H3K27me2	ES-WT	59372399	32834
H3K27me2	ES-Y641F	41090938	19139
H3K27me2	ES-Y641F	39997328	23864
H3K27me2	24h diff-WT	78733451	18553
H3K27me2	24h diff-WT	68050715	20331
H3K27me2	MB-C2C12	33856483	7716
H3K27me2	MB-C2C12	27201472	9006
H3K27me1	ES-WT	36870938	18957
H3K27me1	ES-WT	18153597	12144
H3K27me1	ES-Y641F	32691043	4232
H3K27me1	ES-Y641F	22822845	3520
H3K27me1	24h diff-WT	32216315	20901
H3K27me1	24h diff-WT	31933394	23548
H3K27ac	ES-WT	43436134	44845
H3K27ac	ES-WT	41688403	42143
H3K27ac	ES-Y641F	43905499	42202
H3K27ac	ES-Y641F	49031126	33567
H3K27ac	24h diff-WT	37546234	33954
H3K27ac	24h diff-WT	48153389	34338
H3K4me1	ES-Y641F	53543813	72809
H3K4me1	EB8-WT	25589539	42830
H3K4me1	ES-WT	29682375	69649
Ezh2	ES-WT	23447233	14945
Ezh2	ES-WT	69676607	32644
Ezh2	ES-Y641F	19010314	17842
Ezh2	ES-Y641F	93812560	31223

mRNA-seq	# of unique reads
ES-WT-serum	62795837
ES-WT-serum	59777949
ES-WT-serum	90596323
ES-Y641F-serum	57690908
ES-Y641F-serum	60917762
ES-Y641F-serum	69993587
ES-WT-2i	68140722
ES-WT-2i	58805718
ES-WT-2i	54745595
ES-Y641F-2i	56019864
ES-Y641F-2i	49711497
ES-Y641F-2i	34013223
24h diff-WT	37262614
24h diff-WT	43448505
24h diff-WT	49977650
EB8-WT	50577438
EB13-WT	38842344
EB8-Y641F	50019615
EB13-Y641F	50549941

Juan et al. Fig.S1

Figure S1 (related to Figure 1). H3K27 Methylation Antibody Specificity and Number of Sequencing Reads Across ChIP-seq and mRNA-seq Replicates

(A) The specificity of antibodies against different degrees of H3K27 methylation was tested via dot-blot assay (left panel) and immunoprecipitated ESC lysates (right panel).

(B) Number of unique sequencing reads in individual sample replicates of ChIP-seq (left panel) and mRNA-seq (right panel).

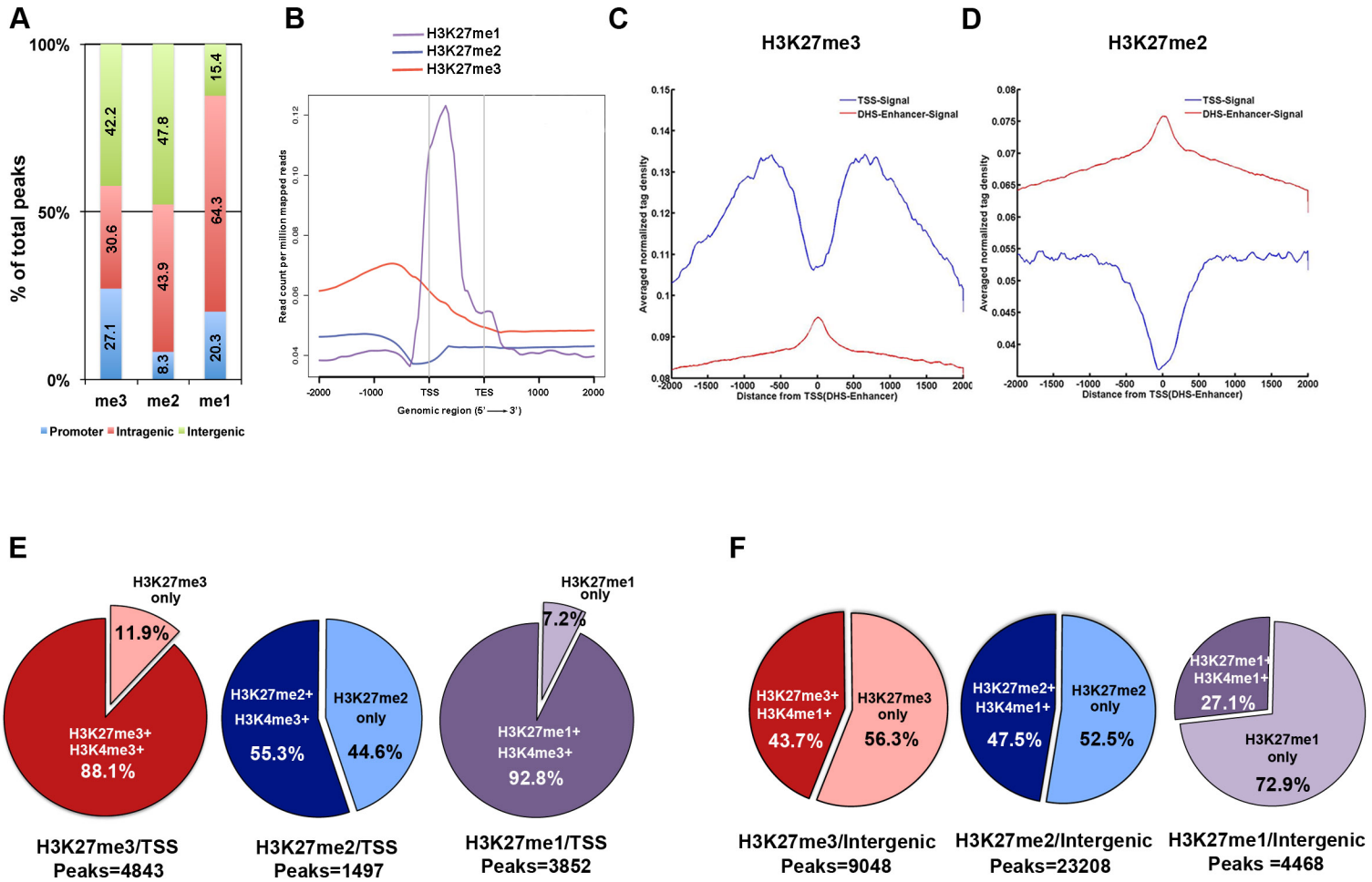

Juan et al. Fig. S2

Figure S2 (related to Figure 1). Distinct H3K27 Methylation States Are Enriched at Functionally Defined Genomic Regulatory Regions

(A) Bar plot showing percentage of H3K27me3, H3K27me2, and H3K27me1 peaks distributed in promoter, intragenic, and intergenic regions.

(B) Read count per million mapped reads of H3K27me3, H3K27me2, and H3K27me1 from 2Kb upstream of TSS to 2Kb downstream of transcription end site (TES).

(C) and (D) Averaged normalized tag density profiles of H3K27me3 (C) or H3K27me2 (D) at transcriptional start site (TSS) (blue line) versus prospective DNase hypersensitive sites (DHS) (red line) enhancer regions.

(E) Percentage of co-occupancy of H3K4me3 and H3K27me3 (left panel), H3K27me2 (middle panel), and H3K27me1(right panel) at TSS regions.

(F) Percentage of co-occupancy of H3K4me1 and H3K27me3 (left panel), H3K27me2 (middle panel), and H3K27me1(right panel) at intergenic regions.

(G) through (I) Gene ontology (GO) based on biological processes for genes occupied by H3K27me3 (G), H3K27me2 (H), or H3K27me1 (I) at TSS regions divided by lower expression (RPKM<1) or higher expression (RPKM>1).

A

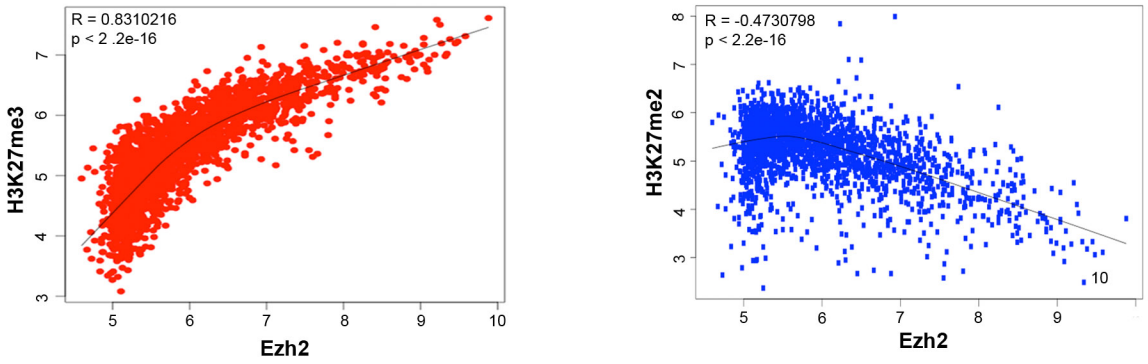

B

E14_me3	E14_me2
GGGGCG	GGGCGG
CGCCCC	CCGCCC
GCCGCC	CCCCGC
CCCCGC	GGGGCG
GCGGGG	GGCGGG
GGCGGC	GCGGGG
CCGCCC	CCCGGG
GGGCGG	CGCCCC
GCCCCG	CCCGCC
CGGGGC	CGGGGC
CCCGCC	CCGGGG
GGCGGG	GCCCCG
GCCCGG	GCCGGG
CCGGGG	CCGGGC
CCCGGC	CCCCGG
GCCGGG	GCCCGG
CCGGGC	CCCGGC
CCCCGG	TCCCGG
CCCGGG	CTGCGG
GGCCGG	CTCCCG
TGCGTG	TGCGTG
CCCCCG	CGGGGA
CGGGGG	CGGGAG
CCGGCC	CACGCA
CCGCCT	CTCCGG

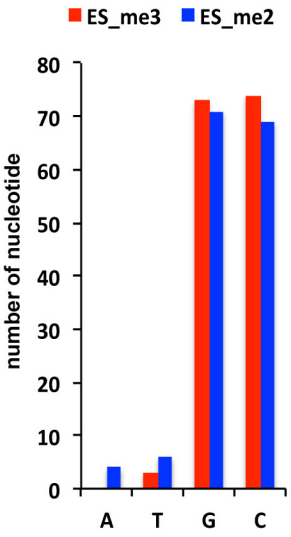

C

me2	me3
RBPj1	RBPj1
EBF1	EBF1
HIF-1b	HIF-1b
Maz	Maz
E2F6	E2F6
E2A	E2A
HRE	Mef2c
c-Myc	BMYB
n-Myc	Gfi1b
AP-1	CHR

D

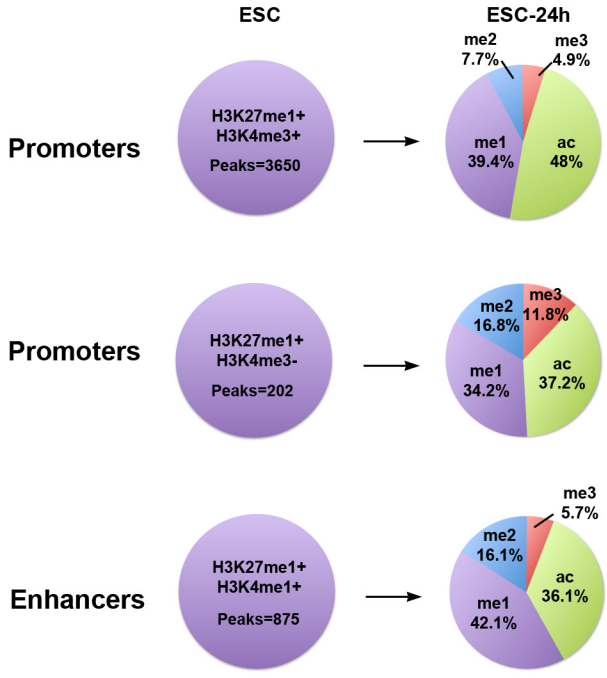

E

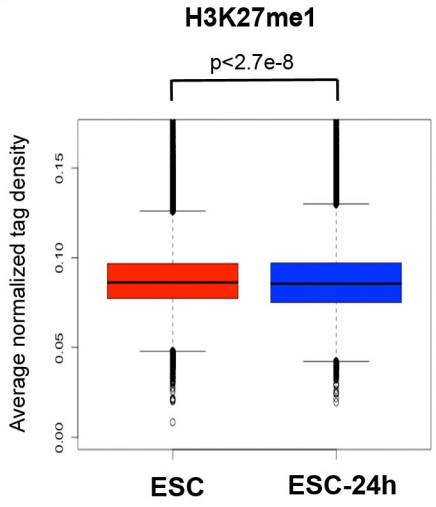

Juan et al. Fig. S3

Figure S3 (related to Figure 1). Ezh2 Preferentially Occupies H3K27me3 Regions

(A) Scatter plots correlation between Ezh2 binding and H3K27me3 occupancy (left panel) and Ezh2 binding and H3K27me2 occupancy (right panel). The R coefficient is determined by Pearson correlation. The p-values are determined by Wilcoxon rank test.

(B) List of top 25% 6-mer sequences within H3K27me3- and H3K27me2-enriched genomic regions (left panel) and total nucleotide count of these 6-mers (right panel)

(C) Top 10 DNA-binding motifs within H3K27me3- or H3K27me2-enriched promoter regions.

(D) Transition of H3K27me1 across H3K4me3$^{+/-}$ promoters and H3K4me1^{+} enhancers in ESCs to different H3K27 states during early ESC differentiation (ESC-24h).

(E) Box plot of H3K27me1 peak intensities for ±5Kb intergenic genomic regions surrounding the summit of each peak at two different ESC developmental stages. P-values were determined by Student's t-test.

A

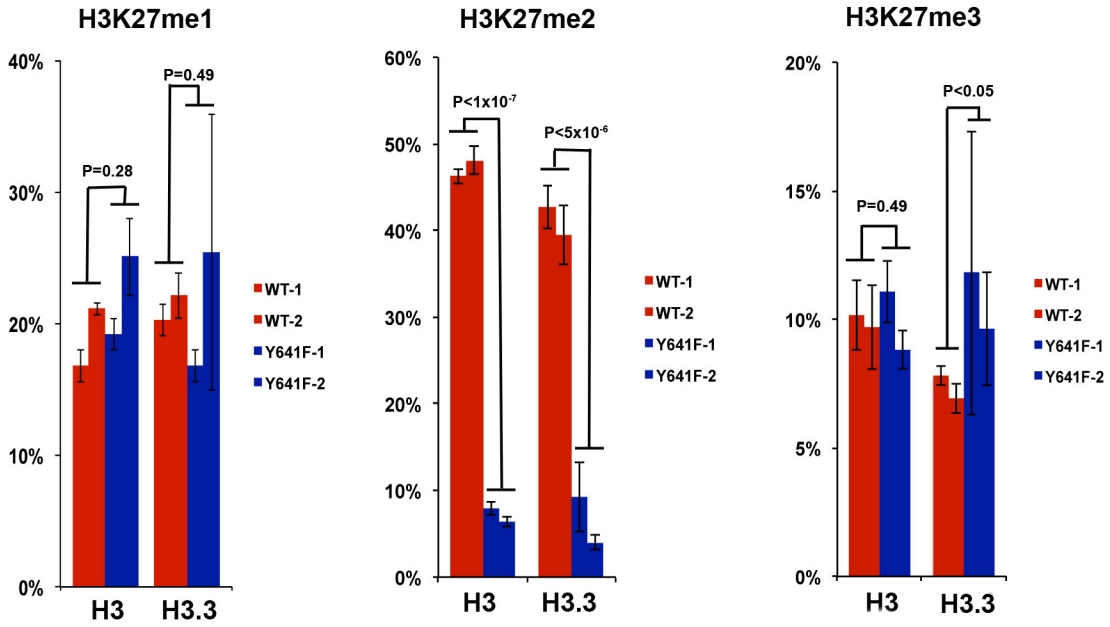

B

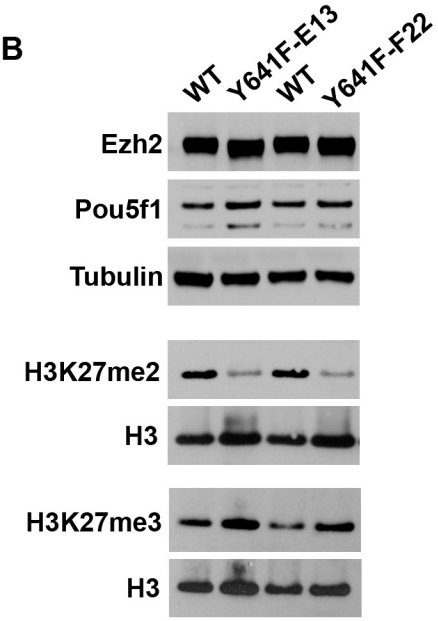

C

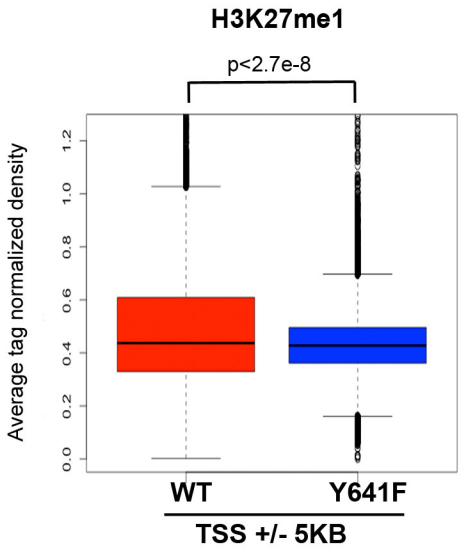

Juan et al. Fig S4

Figure S4 (related to Figure 2). Mass Spectrometry Analysis of H3K27 Methylation in WT and Y641F ESCs and Characterization of Two Additional Y641F ESC Clones

(A) Levels of H3K27me1 (left panel), H3K27me2 (middle panel), and H3K27me3 (right panel) in WT and Y641F ESCs as determined by LC-MS analysis.

(B) Western blot analysis of Ezh2, Pou5f1 and H3K27 methylation in two independent Ezh2-Y641F mutant ESCs (Y641F-E13, Y641F-F22).

(C) Box plot of H3K27me1 peak intensities for genomic regions surrounding (±5Kb) TSS in WT and Y641F ESCs. P-values were determined by Student's t-test.

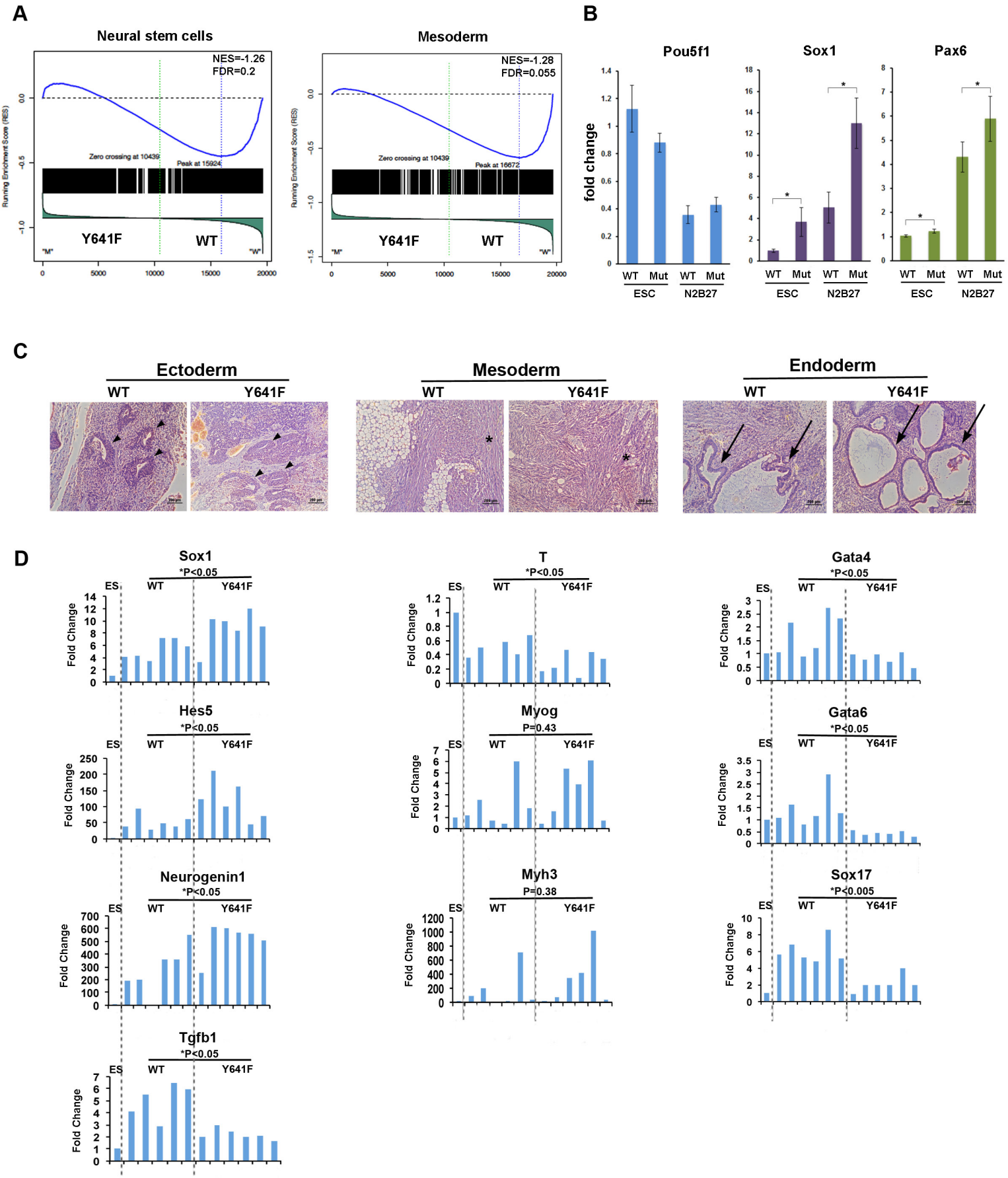

Juan et al. Fig S5

Figure S5 (related to Figure 5). Y641F ESCs Demonstrate a Propensity for Neural Fate Acquisition upon Differentiation

(A) Gene Set Enrichment Analysis (GSEA) for neural stem cell (left panel) and mesodermal (right panel) genes among Y641F and WT ESCs.

(B) RNA expression fold-change of *Pou5f1*, *Sox1*, and *Pax6* in WT and Y641F ESCs cultured for 2 days in either ESC pluripotency or N2B27 media. $^{*}P < 0.05$ (n=3).

(C) Histological H&E staining of WT and Y641F ESCs-derived teratomas documenting ectodermal (left panel), mesodermal (middle panel, stars), and endodermal (right panel) structures. Arrowheads, neural epithelium; stars, skeletal muscle; Arrows: respiratory epithelium.

(D) RNA expression fold-change of *TGF-β1*, neural (*Sox1*, *Hes5*, *Ngn1*), mesodermal (*T*, *Myog*, *Myh3*), and endodermal (*Gata4*, *Gata6*, *Sox17*) transcripts in of WT and Y641F ESCs-derived teratomas.

A

Expression down >1.5 fold in ESC-24h

Kegg pathway terms	P value
mmu04510:Focal adhesion	2.49E-09
mmu04060:Cytokine-cytokine receptor interaction	8.99E-09
mmu04512:ECM-receptor interaction	4.08E-08
mmu04350:TGF-beta signaling pathway	8.83E-08
mmu05200:Pathways in cancer	5.02E-05

B

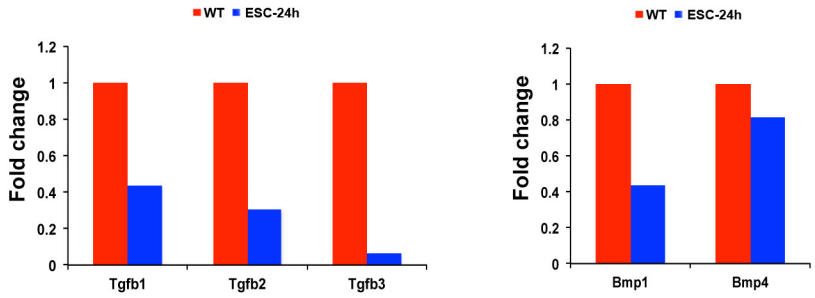

Juan et al. Fig. S6

Figure S6 (related to Figure 6). TGF-β Pathway Repression Occurs during Early ESC Differentiation

(A) Pathway KEGG analysis associated with genes with ≥1.5-fold-decrease in RNA expression in ESC-24h compared to WT ESCs.

(B) RNA expression fold-change (RPKM) from 3 replicates of RNA-seq for TGF-β family members between WT and ESC-24h.

Supplemental Tables

Table S1 Summary of RNA seq and reagents

Table S2 Gene list and GO analysis of H3K27me2 and me3 in the ESC-WT TSS sites (related to Figure S2)

Table S3 Gene list and GO analysis of H3K27me2 and me3 occupied sites in ESC-WT and ESC-24h cells (related to Figure 1)

Table S4 Gene list and GO analysis of sites that reduced me2 in Y641F- increased ac in ESC-24h and sites that increased Y641F and ESC-24h (related to Figure 3 and 4)

Table S5 GO and Kegg pathway analysis of WT vs Y641F RNA expression in ES-serum, ES-2i, EB8, and EB13 (related to Figure 5 and 6)

Supplemental Movie 1 (related to Figure 5)